East European Journal of Physics. 4. 517-526 (2025)
DOI:10.26565/2312-4334-2025-4-53 ISSN 2312-4334

DIELECTRIC CONSTANTS AND TRANSVERSE EFFECTIVE CHARGES IN THE QUINARY ALLOY $Ga_xIn_{1-x}N_ySb_zAs_{1-y-z}$ LATTICE MATCHED TO InAs, GaSb AND GaAs

H. Zerroukhi[1#], H. Abid[1], H. Baaziz[2,3], T. Ghellab[2,3], Z. Charifi[2,3]*
[1]*Applied Materials Laboratory, Research Center, sidi Bel Abbes University, 22000 Algeria*
[2]*Department of Physics, Faculty of Science, University of M'sila, 28000 M'sila, Algeria*
[3]*Laboratory of physics and chemistry of materials, University of M'sila, Algeria*
** Corresponding author e-mail: hakim.baaziz@univ-msila.dz; houari.zerroukhi@univ-sba.dz*
Received July 9, 2025; revised October 21, 2025; accepted October 23, 2025

This study provides a comprehensive theoretical analysis of the dielectric properties and transverse effective charges of the pentanary alloy $Ga_xIn_{1-x}N_ySb_zAs_{1-y-z}$, focusing on compositions that are lattice-matched to InAs, GaSb, and GaAs substrates. The investigation employs the local empirical pseudopotential method (EPM) in conjunction with the virtual crystal approximation (VCA) and the Harrison bond-orbital model to evaluate key parameters, including the static and high-frequency dielectric constants, ionicity, polarity, and transverse effective charge. These computational approaches were chosen due to their ability to accurately describe electronic interactions in complex alloy systems while maintaining computational efficiency. The results demonstrate strong consistency with available experimental data for the constituent binary compounds, reinforcing the reliability of the theoretical framework. Additionally, the study reveals systematic trends in the dielectric behavior as a function of composition, providing insights into the role of atomic substitution in tuning these properties. To the best of our knowledge, this work represents the first detailed theoretical assessment of $Ga_xIn_{1-x}N_ySb_zAs_{1-y-z}$ alloys in this context. While experimental validation remains necessary, our findings establish a valuable theoretical benchmark for future studies and potential applications in optoelectronic and semiconductor device engineering, particularly in the design of advanced infrared detectors and high-frequency electronic components.
Keywords: *EPM; Polarity; Dielectric constants; Transverse effective charge; Lattice matched alloys; Pentanary*
PACS: 77.22.Ch; 78.55.Cr; 71.22.+I; 71.15.Dx; 71.23.-k

1. INTRODUCTION

The integration of III-N-V semiconductors into modern optoelectronic and high-frequency microelectronic devices has gained significant attention due to their unique electronic and optical properties [1]. These materials exhibit direct band gaps [2], high carrier mobilities, and tunable electronic characteristics, making them essential for applications such as infrared photodetectors, laser diodes, and high-speed transistors [3,4]. In particular, they are widely used in fiber-optic communication systems, where the 1.3 μm and 1.5 μm wavelength regimes are critical for minimizing signal attenuation [5]. The incorporation of nitrogen into III-V semiconductors plays a crucial role in band gap engineering, as even small amounts of nitrogen induce a substantial reduction in the band gap [6], thereby allowing for precise control of optical and electronic properties.

Among the various III-N-V compounds, the pentanary alloy $Ga_xIn_{1-x}N_ySb_zAs_{1-y-z}$ presents a promising material system with highly tunable properties while maintaining lattice-matching conditions with widely used substrates such as InAs, GaSb, and GaAs. Ensuring lattice matching is essential for epitaxial growth, as strain-induced defects can significantly degrade the material's electronic transport properties, optical efficiency, and thermal stability. The ability to engineer the band gap and dielectric properties of pentanary alloys while preserving structural compatibility with established semiconductor platforms opens new avenues for the development of advanced optoelectronic devices. Despite their technological potential, pentanary III-N-V alloys remain largely unexplored in terms of their dielectric response and transverse effective charge behavior. While binary and ternary III-V semiconductors have been extensively studied, the complexity introduced by five constituent elements makes direct experimental characterization particularly challenging. This necessitates a rigorous theoretical investigation to systematically analyze the dielectric properties of $Ga_xIn_{1-x}N_ySb_zAs_{1-y-z}$, providing critical insights that can serve as a theoretical foundation for experimental studies and device optimization.

To achieve an accurate and predictive description of the dielectric properties of these alloys, we employ a combination of well-established theoretical approaches. The local empirical pseudopotential method (EPM) is utilized to model electron-ion interactions, providing an effective means of describing the electronic band structure of complex multi-component alloys [7,8]. This method has been extensively validated against experimental data for binary III-V semiconductors, demonstrating its reliability in capturing essential electronic properties. The virtual crystal approximation (VCA) [9] is employed to treat the pentanary alloy as an effective medium, where the electronic properties are approximated as a weighted average of the constituent binaries. This approximation offers a computationally efficient means of estimating key dielectric parameters, ionicities, and transverse effective charges, enabling a predictive framework for understanding composition-dependent variations in material properties. Additionally, Harrison's bond-orbital model [10,11] is incorporated to refine the description of chemical bonding, interatomic interactions, and charge transfer effects. This analytical approach allows the

Cite as: H. Zerroukhi, H. Abid, H. Baaziz, T. Ghellab, Z. Charifi, East Eur. J. Phys. 4, 517 (2025), https://doi.org/10.26565/2312-4334-2025-4-53

calculation of dielectric constants, ionicity, and the transverse effective charge by explicitly accounting for orbital hybridization effects, thereby providing deeper insight into the polarization dynamics and dielectric response of the alloy.

The primary objective of this work is to conduct a comprehensive theoretical analysis of the static and high-frequency dielectric constants, ionicity, polarity, and transverse effective charge of the pentanary alloy $Ga_xIn_{1-x}N_ySb_zAs_{1-y-z}$ while maintaining lattice-matching conditions with InAs, GaSb, and GaAs substrates. The study aims to determine how the dielectric response evolves as a function of alloy composition, how substrate selection influences the transverse effective charge and ionicity, and how these properties can be optimized for optoelectronic applications, particularly in the mid-infrared spectral range. A key aspect of this investigation is to establish quantitative relationships between alloying effects and dielectric behavior, providing fundamental insights into the design of III-N-V materials for advanced photonic and electronic applications. Given the absence of experimental data for pentanary III-N-V alloys, the findings presented in this work serve as a benchmark for future experimental validation and materials engineering efforts.

2. THEORETICAL FORMALISM

To better understand the structural and electronic properties of semiconductor materials, we rely on the interpretation of various experiments, whose coherence depends on an accurate representation of their electronic structures based on band theory. Given the impossibility of solving the Schrödinger equation exactly for an n-body system, approximation methods have been employed to achieve the best possible agreement between calculated and measured values of key quantities such as energy levels and bond lengths. Over the past decades, numerous electronic structure calculation techniques have been developed, particularly empirical methods, which have now become fundamental tools for computing complex structural and electronic properties. These methods also serve as valuable tools for predicting the properties of new materials.

In the empirical pseudopotential approach, the potential of a semiconductor is typically described as the sum of local and nonlocal pseudo-atomic contributions, given by $V = V_L + V_{NL}$. However, in the present study, the nonlocal term (V_{NL}) is neglected. The corresponding pseudopotential Hamiltonian is formulated as $H = (-h/2m)\nabla^2 + V_L(r)$, where the effective potential $V_L(r)$ is expressed as a Fourier expansion in the reciprocal lattice space [7-14]. The lattice parameter of the pentanary alloy $Ga_xIn_{1-x}N_ySb_zAs_{1-y-z}$ obeys the following relationship:

$$a\left(Ga_xIn_{1-x}N_ySb_zAs_{1-y-z}\right) = xya(GaN) + xza(GaSb) + x(1-y-z)a(GaAs) \\ +(1-x)ya(InN) + (1-x)za(InSb) + (1-x)(1-y-z)a(InAs) \quad (1)$$

Where (a(GaN)), (a(GaAs)), (a(GaSb)), (a(InN)), (a(InAs)), and (a(InSb)) represent the lattice parameters of the binary constituents forming the GaInNAsSb alloy, their values are determined based on Vegard's law [12,13].

Utilizing the virtual crystal approximation (VCA) [14], the pseudopotential form factors for the alloy can be formulated as a sum of nonlinear contributions:

$$V^{s,a}_{Ga_xIn_{1-x}N_ySb_zAs_{1-y-z}} = xyV^{s,a}_{GaN} + xzV^{s,a}_{GaSb} + x(1-y-z)V^{s,a}_{GaAs} \\ +(1-x)yV^{s,a}_{InN} + (1-x)zV^{s,a}_{InSb} + (1-x)(1-y-z)V^{s,a}_{InAs} \quad (2)$$

Where $V^{s,a}$ are the symmetric and antisymmetric pseudopotential form factors at the reciprocal lattice vector G(111), (see Table 1) optimized using the nonlinear least-squares method [15].

Table 1. Presents the optimized local pseudopotential form factors at the Γ, X, and L high-symmetry points of the Brillouin zone (in q^{Ry}) for the relevant binary compounds. Additionally, the corresponding lattice constants (in nd) utilized in the calculations are provided

Compound	Form factors						Lattice constant Å
	Vs(3)	Vs(8)	Vs(11)	Va(3)	Va(4)	Va(11)	
GaAs	-0.239833	0.012600	0.059625	0.060536	0.050000	0.010000	5.653 [a]
InAs	-0.182147	0	0.047107	0.094714	0.05	0.03	6.058 [a]
GaSb	-0.191206	0.005	0.043533	0.04534	0.03	0	6.118 [a]
InSb	-0.201822	0.01	0.028443	0.064645	0.03	0.015	6.4794 [b]
GaN	-0.346925	0.161439	-0.016000	0.200000	0.211824	0.135	4.4878 [c]
InN	-0.328532	0.091201	0.003930	0.320000	- 0.033147	-0.006892	4.9868 [c]

[a] ref. [16]; [b] ref. [17]; [c] ref. [18].

Table 2. The calculated direct and indirect band-gaps energy (in ^{eV}) of our binaries in comparison with the experimental and others works ones

Compound	Band-gap energy (eV)					
	E_g^{Γ}		E_g^{x}		E_g^{L}	
	Exp. Others	Our cal.	Exp. Others	Our cal.	Exp. Others	Our cal.
GaAs	1.424[a]	1.421	1.81[a]	1.814	1.72[a]	1.722
InAs	0.36[b]	0.324	1.37[b]	1.374	1.07[b]	1.072
GaSb	0.725[c]	0.727	1.03[d]	1.015	0.761[d]	0.778
InSb	0.18[b]	0.174	1.63[b]	1.63	0.93[b]	0.93
GaN	3.2[e]	3.20	4.7[e]	4.602	6.2[e]	6.045
InN	0.7[f]	0.778	2.51[g]	2.518	5.82[h]	5.825

[a] ref. [19]; [b] ref. [20]; [c] ref. [21]; [d] ref. [22]; [e] ref. [7]; [f] ref. [23]; [g,h] ref. [8].

The eigenvalue problem in this study is characterized by a 136×136 matrix. The pseudopotential form factors are determined by the magnitudes of the reciprocal lattice vectors (G). To ensure computational accuracy, a cutoff value of $|G|^2 = 11(2\pi/a)^2$ is applied.

The lattice-matching condition for the pentanary alloy $Ga_xIn_{1-x}N_ySb_zAs_{1-y-z}$ on InAs, GaSb and GaAs substrates is obtained from Equation (1) and can be expressed as follows:

$$y = \frac{a\,sub + 0.405\,x - 0.4214\,z - 0.0436\,xz - 6.058}{-(0.094x + 1.0712)} \tag{3}$$

Where $a_{sub} = a_{InAs} = 6.058$ Å for InAs substrate, $a_{sub} = a_{GaSb} = 6.118$ Å for GaSb substrate and $a_{sub} = a_{GaAs} = 5.653$ Å for GaAs substrate.

By employing the Herve and Vandamme expression [22], the refractive index *n* was determined, which is essential for designing quantum well lasers and solar cell applications. This expression is valid in the low-frequency limit $\omega \ll \omega_0$, where ω_0 represents the ultraviolet resonance frequency.

$$n = \sqrt{1 + \left(\frac{A}{E_g + B}\right)^2} \tag{4}$$

where E_g is the fundamental band-gap energy and A=13.6 eV and B =3.4 eV.

The optical high-frequency dielectric constant (ε_∞) is given by the square of the refractive index, n^2 [23].

$$\varepsilon_\infty = n^2 \tag{5}$$

Using the Harrison model [24], the static dielectric constant ε_0 can be expressed in terms of the optical high-frequency dielectric constant (ε_∞) through the following relation:

$$\frac{\varepsilon_0 - 1}{\varepsilon_\infty - 1} = 1 + v \tag{6}$$

Where v is given by [25],

$$v = \frac{\alpha_p^2\,(1 + 2\alpha_c^2)}{2\alpha_c^4} \tag{7}$$

The covalency α_c of the material under study is associated with its polarity α_p through the following relationship:

$$\alpha_c = (1 - {\alpha_p}^2)^{1/2} \tag{8}$$

The polarity α_p is defined by Vogl [25] as

$$\alpha_p = \frac{-V^a(3)}{V^s(3)} \tag{9}$$

$V^s(3)$ and $V^a(3)$ represent the symmetric and antisymmetric pseudopotential form factors at the reciprocal lattice vector G(111). The transverse effective charge (e_T^*) is computed using the following expression [26]:

$$2e_T^* = -\Delta_Z^* + \frac{8\alpha_p}{1 + {\alpha_p}^2} \tag{10}$$

Where

$$\Delta_z^* = xz_{Ga}^* + (1 - x)z_{In}^* - yz_N^* - zz_{Sb}^* - (1 - y - z)z_{As}^* \tag{11}$$

In last, we have the iconicity f_i given by,

$$f_i = 1 - {\alpha_c}^3 \tag{12}$$

3. NUMERICAL RESULTS

Allowed lattice-matching relations between x, y, and z for the $Ga_xIn_{1-x}N_ySb_zAs_{1-y-z}$ alloy with the substrates GaAs, InAs, and GaSb are shown in Figures 1a, 1b, and 1c. These figures provide critical insights into the compositional constraints required to achieve lattice-matching with different substrates, an essential factor in optimizing semiconductor heterostructures for device applications.

The study of static and high-frequency dielectric constants, transverse effective charge, and ionicity in multi-component alloys such as GaInNAsSb is crucial in modern material research. A deep understanding of these parameters enables the design and optimization of materials for semiconductor applications, leading to technological advancements in optoelectronic devices, high-speed electronics, and infrared photodetectors. This motivates our investigation into these fundamental properties.

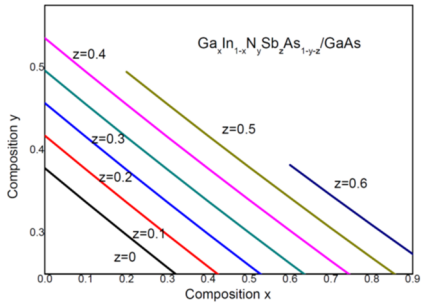

Figure 1a. Allowed lattice-matching relations between x, y, and z for the $Ga_xIn_{1-x}N_ySb_zAs_{1-y-z}$ with the substrate GaAs

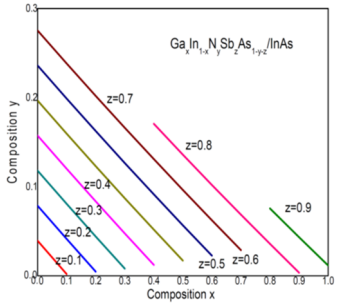

Figure 1b. Allowed lattice-matching relations between x, y, and z for the $Ga_xIn_{1-x}N_ySb_zAs_{1-y-z}$ with the substrate InAs

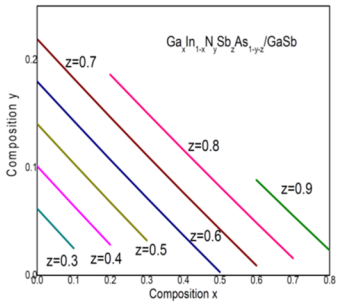

Figure 1c. Allowed lattice-matching relations between x, y, and z for the $Ga_xIn_{1-x}N_ySb_zAs_{1-y-z}$ with the substrate GaSb

Table 3. Optical static dielectric constant (ε_0), optical high-frequency dielectric constant (ε_∞), and transverse effective charge (e_T^*) of binaries of interest

Compound	ε_0		ε_∞		e_T^*	
	Exp.	Our cal.	Exp.	Our cal.	Exp.	Our cal.
GaAs	12.9[a]	9.78	10.9[a]	8.95	2.07[b]	1.95
InAs	15.15[a]	22.66	12.3[c]	14.33	2.53[c]	2.63
GaSb	15.7[a]	12.85	14.4[c]	11.86	2.15[c]	1.90
InSb	16.8[a]	18.05	15.7[c]	15.48	2.42[c]	2.16
GaN	9.7[d]	7.16	5.30[d]	5.25	2.51[e]	2.53
InN	8.40[f]	8.43	8.4[f]	7.58	3.04[e]	2.03

[a] ref. [27]; [b] ref. [28]; [c] ref. [29]; [d] ref. [26]; [e] ref. [30]; [f] ref. [31]

Table 3 presents the calculated values of the optical static dielectric constant (ε_0), optical high-frequency dielectric constant (ε_∞), and transverse effective charge (e_T^*) for the relevant binary compounds, compared with available experimental data. The computed values generally follow the expected trend, where compounds with higher dielectric constants exhibit stronger polarization and lower band gaps. GaAs, InAs, and GaSb exhibit relatively high (ε_0), indicating strong electronic polarizability, while GaN and InN have significantly lower values due to their wider band gaps. The agreement between computed and experimental values validates the accuracy of our theoretical model.

The transverse effective charge reflects the bond ionicity and charge transfer characteristics of the materials. The results indicate that InAs and InSb exhibit higher (e_T^*) values than GaAs and GaSb, suggesting a greater degree of ionicity and charge asymmetry in their bonding. GaN and InN show relatively high transverse effective charges, consistent with their polar nature and strong ionicity. The theoretical values are in good agreement with experimental references, confirming the reliability of our computational framework. Minor discrepancies, such as a slight underestimation of (ε_0) for GaAs and overestimation for InSb, can be attributed to computational approximations, particularly in electron-phonon interactions.

The binary dielectric properties in Table 3 provide a foundation for understanding the behavior of GaInNAsSb. By tuning the composition (x, y, z), the dielectric response can be engineered for specific applications, such as optimizing (ε_∞) for better light absorption and carrier confinement in quantum wells, adjusting (e_T^*) to enhance electronic polarization and charge transport in infrared and terahertz applications, and controlling dielectric screening for high-speed transistors and photodetectors. The results obtained in this study demonstrate strong agreement with experimental data, confirming the suitability of the theoretical approach in predicting dielectric and charge transport properties in complex semiconductor alloys.

Figures 2 and 3 illustrate the calculated optical static dielectric constant (ε_0) and the high-frequency dielectric constant (ε_∞) for the pentanary alloy $Ga_xIn_{1-x}N_ySb_zAs_{1-y-z}$, considering two different lattice-matching conditions: InAs and GaSb. These figures provide valuable insight into the role of nitrogen incorporation on the dielectric properties of the material.

The static dielectric constant (ε_0) shown in Figure 2 exhibits a monotonic increase with increasing nitrogen content (y) in the range ($0 \leq y \leq 0.218$). This trend can be attributed to the larger polarizability of the alloy as more nitrogen is incorporated, which alters the local bonding environment and enhances the dielectric response. The increase in (ε_0) is evident for both lattice-matching conditions, but the GaSb-matched alloy exhibits a slightly higher dielectric constant than the InAs-matched one. This difference suggests that GaSb exerts a stronger influence on dielectric screening, likely due to its effect on strain and electronic band structure.

In contrast, Figure 3 shows that the high-frequency dielectric constant (ε_∞) decreases as the nitrogen content increases. This decline suggests that the electronic band structure is modified in a way that reduces the material's ability to respond to high-frequency optical fields. Interestingly, at low nitrogen concentrations ($y<0.138$), the GaSb-matched alloy has a slightly higher (ε_∞) than the InAs-matched one. However, beyond ($y= 0.138$), an opposite trend emerges where

the InAs-matched alloy exhibits a larger (ε_∞) than the GaSb-matched alloy. This crossover behavior indicates a transition in the dominant dielectric response mechanism, highlighting the impact of substrate selection on optical properties.

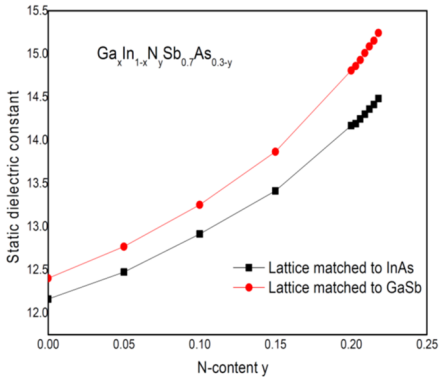

Figure 2. Static dielectric constant ε_0 in $Ga_xIn1_{-x}N_ySb_{0.7}As_{0.3-y}$ lattice matched to InAs and GaSb as a function of various N-content

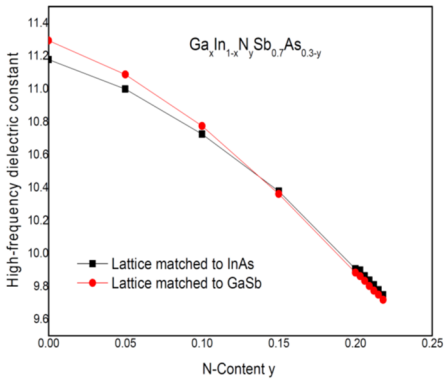

Figure 3. High-frequency dielectric constant ε_∞ in $Ga_xIn_{1-x}N_ySb_{0.7}As_{0.3-y}$ lattice matched to InAs and GaSb as a function of various N-content

The observed trends in (ε_0) and (ε_∞) can be understood through the interplay of nitrogen incorporation, strain effects from the substrate, and modifications in the electronic band structure. The increase in (ε_0) with nitrogen content is a direct consequence of increased lattice distortion and bond polarity. The decline in (ε_∞) suggests a reduction in free carrier screening at optical frequencies, which may be linked to increased localization effects introduced by nitrogen. Additionally, the switching behavior of (ε_∞) at (y = 0.138) emphasizes the substrate's role in influencing the dielectric response, affecting both static and optical properties.

These findings demonstrate the significant impact of nitrogen incorporation and substrate selection on the dielectric properties of $Ga_xIn_{1-x}N_ySb_zAs_{1-y-z}$. The variations in ($\varepsilon_0$) and ($\varepsilon_\infty$) highlight the potential for tailoring these properties for optoelectronic applications. The observed trends could be particularly relevant in designing materials with optimized dielectric screening and optical performance for infrared and telecommunication applications.

From the fit of the static and high-frequency dielectric constants data by a least-squares procedure, the expressions of the computed parameters are:

$$\varepsilon_0 = 12.175 + 4.24y + 28.51y^2 \text{ for } Ga_xIn_{1-x}N_ySb_{0,7}As_{0,3-y}/InAs \quad (13.a)$$

$$\varepsilon_0 = 12.432 + 3.84y + 40.63y^2 \text{ for } Ga_xIn_{1-x}N_ySb_{0,7}As_{0,3-y}/GaSb \quad (13.b)$$

$$\varepsilon_\infty = 11.178 - 2.74y - 17.58y^2 \text{ for } Ga_xIn_{1-x}N_ySb_{0,7}As_{0,3-y}/InAs \quad (14.a)$$

$$\varepsilon_\infty = 11.301 - 3.68y - 16.66y^2 \text{ for } Ga_xIn_{1-x}N_ySb_{0,7}As_{0,3-y}/GaSb \quad (14.b)$$

From the least-squares fitting of the calculated dielectric constant data, the obtained quadratic expressions reveal distinct behaviors for the static dielectric constant (ε_0) and high-frequency dielectric constant (ε_∞) as functions of nitrogen content (y) in $Ga_xIn_{1-x}N_ySb_{0.7}As_{0.3-y}$ alloys lattice-matched to GaSb and InAs. The fitted expressions for (ε_0) indicate a strong non-linear dependence on nitrogen content, as evidenced by the significant upward bowing parameters. The bowing parameter for (ε_0) is larger for the GaSb-matched alloy (+40.63) compared to the InAs-matched alloy (+28.51), suggesting that nitrogen incorporation strongly enhances the static dielectric response, likely due to increased bond ionicity and polarization effects. The more pronounced bowing in the GaSb-matched alloy indicates a stronger influence of nitrogen on dielectric screening, which may be attributed to the different strain conditions induced by the lattice-matching requirement. The static dielectric constant varies between 12.40 and 15.24 for the GaSb-matched alloy, whereas for the InAs-matched alloy, it ranges from 12.16 to 14.48. The slightly higher values in the GaSb case suggest stronger dielectric screening, which could impact carrier mobility and optical absorption properties in optoelectronic applications.

Unlike (ε_0), the high-frequency dielectric constant (ε_∞) exhibits a downward bowing with nitrogen incorporation, with nearly identical bowing parameters of -16.66 for the GaSb-matched alloy and -17.58 for the InAs-matched alloy. This downward bowing indicates that increasing nitrogen content reduces the material's ability to respond to optical frequencies, likely due to modifications in the electronic band structure, particularly a reduction in the bandgap and an increase in carrier localization effects. The similar bowing parameters for both substrate conditions suggest that the primary factor influencing (ε_∞) is the electronic structure modification induced by nitrogen, rather than substrate-related strain effects. The high-frequency dielectric constant decreases from 11.29 to 9.71 for the GaSb-matched alloy, while for the InAs-matched alloy, it ranges from 11.17 to 9.74. The reduction in (ε_∞) with increasing nitrogen content is consistent with the expected bandgap widening and reduced free carrier screening, which has direct implications for optical applications.

The observed differences in (ε_0) and (ε_∞) between the GaSb-matched and InAs-matched alloys highlight the role of ionicity in dielectric behavior. Higher ionicity leads to stronger dipole interactions, affecting dielectric screening and optical response. This is particularly relevant for laser devices and infrared detectors, where dielectric properties directly

influence carrier recombination rates and absorption spectra. Additionally, the transverse effective charge plays a crucial role in the electromechanical coupling of the material. Since (ε_∞) is related to the dynamic response of the lattice to external perturbations, its behavior provides valuable insights into how the alloy interacts with electromagnetic fields, making it critical for designing high-performance optoelectronic and electro-optic devices.

The quadratic fitting expressions provide a comprehensive understanding of the evolution of dielectric properties in $Ga_xIn_{1-x}N_\gamma Sb_{0.7}As_{0.3-y}$ alloys. The strong upward bowing in (ε_0) emphasizes enhanced dielectric screening due to nitrogen incorporation, whereas the downward bowing in (ε_∞) suggests reduced optical response at higher nitrogen concentrations. The differences between GaSb-matched and InAs-matched alloys highlight the substrate effect on dielectric behavior, which must be carefully considered for device engineering in optoelectronic applications, such as lasers, infrared photodetectors, and modulators.

The computed ionicity and transverse effective charge for $Ga_xIn_{1-x}N_ySb_{0.7}As_{0.3-y}$ alloys lattice-matched to InAs and GaSb exhibit an increasing trend with nitrogen content (y) up to 0.218, as shown in Figures 4 and 5. The steady increase in ionicity with increasing (y) suggests that the incorporation of nitrogen enhances the degree of ionicity in the alloy. This behavior can be attributed to the introduction of highly electronegative nitrogen atoms, which alter the charge distribution and strengthen the ionic character of chemical bonds. The ionicity values for the GaSb-matched alloy are systematically higher than those of the InAs-matched alloy, indicating that GaSb provides a more pronounced ionic environment compared to InAs. This difference can be linked to the larger electronegativity contrast in the GaSb system, leading to stronger dipolar interactions and modifications in the electronic band structure.

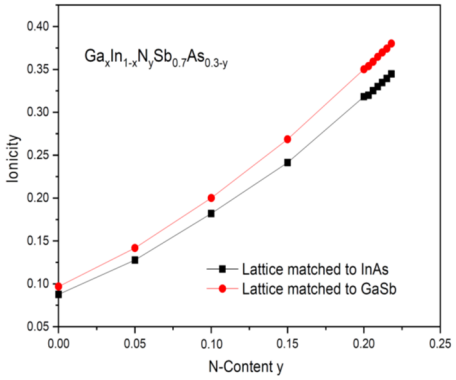

Figure 4. Ionicity in $Ga_xIn_{1-x}N_ySb_{0.7}As_{0.3-y}$ lattice matched to InAs and GaSb as a function of various N-content

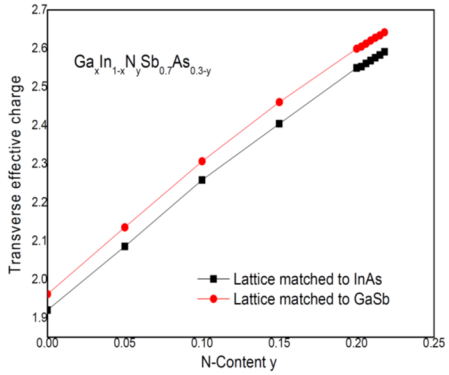

Figure 5. Transverse effective charge in $Ga_xIn_{1-x}N_ySb_{0.7}As_{0.3-y}$ lattice matched to InAs and GaSb as a function of various N-content

Similarly, the transverse effective charge also increases with nitrogen incorporation, emphasizing the role of nitrogen in modulating the electromechanical response of the material. The observed trend suggests that nitrogen atoms introduce additional polarizability in the alloy, thereby enhancing its response to external electric fields. The GaSb-matched alloy consistently exhibits a higher transverse effective charge than the InAs-matched counterpart, reinforcing the idea that the host lattice plays a crucial role in determining the material's electromechanical coupling. This increasing behavior of transverse effective charge is essential for understanding the dielectric screening and phonon interactions within the alloy system, which have direct implications for optoelectronic and high-frequency applications.

The fitted analytical expressions obtained through the least-squares method provide quantitative descriptions of these trends, allowing for predictive modeling of ionicity and transverse effective charge as functions of nitrogen content. The observed variations highlight the fundamental impact of nitrogen incorporation on the dielectric and electromechanical properties of $Ga_xIn_{1-x}N_\gamma Sb_{0.7}As_{0.3-y}$ alloys. These findings are particularly relevant for applications where precise control over ionicity and electromechanical coupling is required, such as infrared photodetectors, high-performance laser devices, and electro-optic modulators.

$$fi = 0.087 + 0.71y + 2.12y^2 \text{ for } Ga_xIn_{1-x}N_ySb_{0,7}As_{0,3-y}/InAs \quad (15.a)$$

$$fi = 0.096 + 0.8y + 2.27y^2 \text{ for } Ga_xIn_{1-x}N_ySb_{0,7}As_{0,3-y}/GaSb \quad (15.b)$$

$$e_T^* = 1.917 + 3.59y - 2.28y^2 \text{ for } Ga_xIn_{1-x}N_ySb_{0,7}As_{0,3-y}/InAs \quad (16.a)$$

$$e_T^* = 1.96 + 3.74y - 2.8y^2 \text{ for } Ga_xIn_{1-x}N_ySb_{0,7}As_{0,3-y}/GaSb \quad (16.b)$$

The computed expressions for ionicity (f_i) and transverse effective charge (e_T^*) provide valuable insights into the dielectric and electromechanical properties of $Ga_xIn_{1-x}N_ySb_{0,7}As_{0,3-y}$ alloys. As observed from equations (15.a) to (16.b), the alloy lattice-matched to GaSb exhibits slightly higher ionicity than its InAs-matched counterpart. This can be attributed to the stronger electronegativity contrast between Ga and Sb atoms, which enhances the ionic nature of chemical bonds in the GaSb lattice. The presence of nitrogen further amplifies this effect, as its high electronegativity increases the polarity of the bonding environment. The quadratic dependence of ionicity on nitrogen content (y) indicates a nonlinear enhancement of ionic character, suggesting that nitrogen plays a crucial role in modifying the alloy's electronic charge

distribution. The larger bowing parameter in the GaSb-matched alloy (+2.27) compared to the InAs-matched alloy (+2.12) reinforces the idea that the host lattice composition significantly influences the ionicity of the material.

Similarly, the transverse effective charge (e_T^*) exhibits a systematic increase with nitrogen incorporation in both alloys, further supporting the role of nitrogen in modulating the electromechanical response of the system. The presence of a negative quadratic term in equations (16.a) and (16.b) suggests that at higher nitrogen concentrations, the rate of increase in transverse effective charge slows down, likely due to saturation effects in charge redistribution. Notably, the GaSb-matched alloy consistently displays a higher transverse effective charge than the InAs-matched alloy, which can be linked to the differences in dielectric screening and bonding strength between the two lattice-matched structures. The stronger dipolar interactions in the GaSb lattice contribute to a greater electromechanical response, making it a more favorable candidate for applications requiring high dielectric tunability and efficient phonon coupling.

Expanding the analysis to the pentanary alloy $Ga_xIn_{1-x}N_ySb_{0.7}As_{0.3-y}$ lattice-matched to GaAs, the study examines the variations in ionicity and transverse effective charge over the nitrogen composition range (y = 0.16) to (0.416) for different arsenic proportions (z = 0.1, 0.2, 0.3, 0.4). These findings provide a deeper understanding of how nitrogen and arsenic jointly influence the electronic properties of the alloy, offering crucial information for optimizing its optoelectronic performance. The interplay between these elements determines the material's dielectric behavior and electromechanical coupling, which are essential parameters for applications in infrared photodetectors, high-frequency transistors, and laser devices.

The calculated optical static dielectric constant (ε_0) and high-frequency dielectric constant (ε_∞) for various nitrogen (N) contents in the pentanary alloy $Ga_xIn_{1-x}N_ySb_zAs_{1-y-z}$, lattice-matched to GaAs, are presented in Figures 6 and 7. Their analytical expressions are given by:

$$\varepsilon_0 = 13.92 - 31.38y + 95.64y^2 \text{ for } Ga_xIn_{1-x}N_ySb_{0.1}As_{0.9-y}/GaAs \quad (17.a)$$

$$\varepsilon_0 = 12.32 - 16.54y + 60.97y^2 \text{ for } Ga_xIn_{1-x}N_ySb_{0.2}As_{0.8-y}/GaAs \quad (17.b)$$

$$\varepsilon_0 = 11.33 - 6.72y + 38.05y^2 \text{ for } Ga_xIn_{1-x}N_ySb_{0.3}As_{0.7-y}/GaAs \quad (17.c)$$

$$\varepsilon_0 = 12.90 - 12.11y + 35.84y^2 \text{ for } Ga_xIn_{1-x}N_ySb_{0.4}As_{0.6-y}/GaAs \quad (17.d)$$

$$\varepsilon_\infty = 9.52 + 3.64y - 20.37y^2 \text{ for } Ga_xIn_{1-x}N_ySb_{0.1}As_{0.9-y}/GaAs \quad (18.a)$$

$$\varepsilon_\infty = 9.31 + 5.68y - 23.49y^2 \text{ for } Ga_xIn_{1-x}N_ySb_{0.2}As_{0.8-y}/GaAs \quad (18.b)$$

$$\varepsilon_\infty = 9.16 + 7.65y - 26.47y^2 \text{ for } Ga_xIn_{1-x}N_ySb_{0.3}As_{0.7-y}/GaAs \quad (18.c)$$

$$\varepsilon_\infty = 11.13 - 2.73y - 13.20y^2 \text{ for } Ga_xIn_{1-x}N_ySb_{0.4}As_{0.6-y}/GaAs \quad (18.d)$$

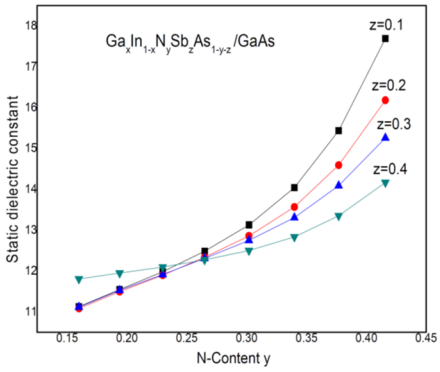

Figure 6. Static dielectric constant ε_0 in $Ga_xIn_{1-x}N_ySb_zAs_{1-y-z}$/GaAs as a function of various N-content with different As-proportion

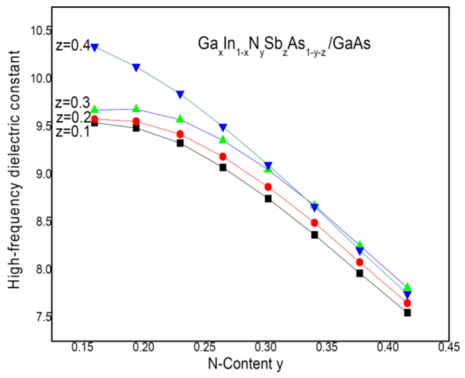

Figure 7. High-frequency dielectric constant ε_∞ in $Ga_xIn_{1-x}N_ySb_zAs_{1-y-z}$/GaAs as a function of various N-content with different As-proportion

The expressions for (ε_0) indicate a strong bowing effect, suggesting significant deviations from a linear interpolation between the parent binaries. Among the compositions studied, $Ga_xIn_{1-x}N_ySb_{0.4}As_{0.6-y}$/GaAs (Eq. 17.d) exhibits a similar behavior to $Ga_xIn_{1-x}N_ySb_{0.7}As_{0.3-y}$/InAs, with a comparable bowing parameter (+35.84) vs. (+28.51). This suggests that, in terms of dielectric response, this composition behaves similarly to an InAs-matched alloy. Conversely, $Ga_xIn_{1-x}N_ySb_{0.3}As_{0.7-y}$/GaAs (Eq. 17.c) exhibits a dielectric behavior comparable to $Ga_xIn_{1-x}N_ySb_{0.7}As_{0.3-y}$/GaSb, as reflected in their nearly identical bowing parameters (+38.05) vs. (+40.63). This suggests that increasing the Sb content in GaAs-matched alloys leads to behavior more characteristic of GaSb-matched alloys.

Unlike (ε_0), the high-frequency dielectric constant decreases with increasing nitrogen content, reflecting reduced electronic polarizability due to shorter bond lengths and increased ionicity. The bowing parameter for (ε_∞) in $Ga_xIn_{1-x}N_ySb_{0.1}As_{0.9-y}$ /GaAs (Eq. 18.a) is comparable to that in $Ga_xIn_{1-x}N_ySb_{0.7}As_{0.3-y}$/InAs) (-20.37) vs. (-17.58), indicating similar electronic screening effects. Conversely, the bowing parameter for (ε_∞) in $Ga_xIn_{1-x}N_ySb_{0.4}As_{0.6-y}$/GaAs (Eq. 18.d)

is close to that of $Ga_xIn_{1-x}N_ySb_{0.7}As_{0.3-y}$/GaSb (-13.20) vs. (-16.66), reinforcing the similarity between these two alloy types.

These results suggest that careful tuning of the composition parameters (x), (y), and (z) allows for the engineering of dielectric properties to match specific applications. For instance, if a material with a higher static dielectric constant is needed (e.g., for high-capacitance device applications), a composition with higher nitrogen and lower arsenic content may be favorable. Conversely, for applications where a lower (ε_∞) is preferred (e.g., to reduce optical losses in high-frequency optoelectronic devices), compositions with lower nitrogen content may be advantageous. Importantly, the close agreement between specific GaAs-matched and InAs- or GaSb-matched alloys implies that a suitable choice of substrate could help mitigate strain effects while maintaining desirable dielectric properties.

The dielectric properties of the pentanary alloy $Ga_xIn_{1-x}N_ySb_zAs_{1-y-z}$, lattice-matched to GaAs, exhibit significant nonlinearity due to strong bowing effects. The similarity in dielectric response between certain compositions and InAs- or GaSb-matched alloys highlights the potential for substrate engineering in device applications. By adjusting the composition parameters, this material system offers a wide range of possibilities for optimizing dielectric constants and transverse effective charges for high-performance optoelectronic and electronic applications.

On the other hand, structural defects and local clustering can greatly influence the dielectric properties of complex pentanary alloys. Defects such as vacancies and lattice dislocations disrupt the periodicity of the crystal structure, leading to the formation of localized electronic states and modifications in the electronic and ionic components of the dielectric constant. At the same time, the local clustering of atoms such as nitrogen or antimony causes compositional inhomogeneity and local strains, resulting in spatial variations in polarization. These effects produce nonuniformities in dielectric properties and deviations from the ideal values predicted by the Virtual Crystal Approximation (VCA), emphasizing the importance of considering real structural defects when comparing theoretical results with experimental data.

Figures 8 and 9 illustrate the computed ionicity f_i and transverse effective charge e_T^* in $Ga_xIn_{1-x}N_ySb_zAs_{1-y-z}$ lattice matched to GaAs as a function of nitrogen content (y) over the range 0.16–0.416 for different arsenic proportions. The fitted data obtained using the least-squares method yield the following analytical expressions:

$$fi = 0.063 + 0.28y + 2.36y^2 \quad (19.a)$$

$$fi = 0.064 + 0.25y + 2.17y^2 \quad (19.b)$$

$$fi = 0.064 + 0.23y + 2y^2 \quad (19.c)$$

$$fi = 0.062 + 0.22y + 1.84y^2 \quad (19.d)$$

$$e_T^* = 1.535 + 4.52y - 3.27y^2 \quad (20.a)$$

$$e_T^* = 1.551 + 4.21y - 2.79y^2 \quad (20.b)$$

$$e_T^* = 1.561 + 3.94y - 2.40y^2 \quad (20.c)$$

$$e_T^* = 1.564 + 3.73y - 2.09y^2 \quad (20.d)$$

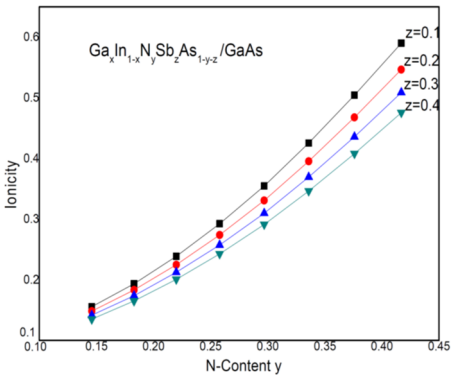

Figure 8. Ionicity in $Ga_xIn_{1-x}N_ySb_zAs_{1-y-z}$ lattice matched to GaAs as a function of various N-content with different As-proportion

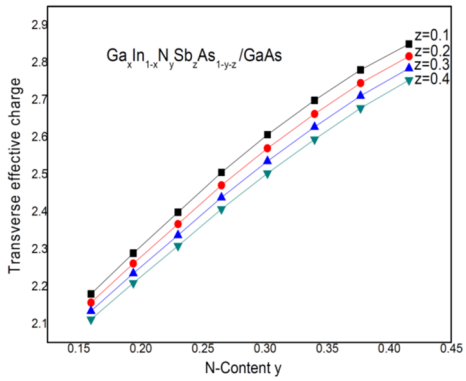

Figure 9. Transverse effective charge in $Ga_xIn_{1-x}N_ySb_zAs_{1-y-z}$ lattice matched to GaAs as a function of various N-content with different As-proportion

The results show a nonlinear increase in ionicity as nitrogen content increases. This is expected because nitrogen, being more electronegative than arsenic and antimony, enhances the ionic character of the bonds in the alloy. The higher the nitrogen incorporation, the greater the charge separation between cations and anions, leading to a more pronounced ionicity.

The transverse effective charge also increases with nitrogen content but exhibits a downward curvature at higher *y* values. This suggests that while nitrogen initially enhances charge transfer effects due to bond polarity, at higher concentrations, structural distortions or charge redistribution effects may counteract this trend. Such behavior is crucial for understanding the dielectric response of these alloys, which impacts their optical and electronic applications.

By comparing these fitted expressions with those obtained for $Ga_xIn_{1-x}N_ySb_zAs_{1-y-z}$ lattice matched to other substrates (InAs and GaSb), notable similarities emerge. The ionicity behavior of $Ga_xIn_{1-x}N_ySb_{0.2}As_{0.8-y}$ lattice matched to GaAs (Eq. 19.b) closely resembles that of $Ga_xIn_{1-x}N_ySb_{0.7}As_{0.3-y}$ lattice matched to InAs (Eq. 15.a). Similarly, the ionicity of $Ga_xIn_{1-x}N_ySb_{0.1}As_{0.9-y}$ lattice matched to GaAs (Eq. 19.a) is comparable to that of $Ga_xIn_{1-xNySb0.7}As_{0.3-y}$ lattice matched to GaSb (Eq. 15.b). These trends indicate that the ionicity in certain GaAs-lattice-matched alloys follows a pattern similar to that of InAs- and GaSb-matched counterparts, suggesting that the As/Sb ratio plays a crucial role in determining bond character.

The transverse effective charge in $Ga_xIn_{1-x}N_ySb_{0.3}As_{0.7-y}$ lattice matched to GaAs (Eq. 20.c) behaves similarly to that of $Ga_xIn_{1-x}N_ySb_{0.7}As_{0.3-y}$ lattice matched to InAs (Eq. 16.a). Likewise, e^*_T in $Ga_xIn_{1-x}N_ySb_{0.2}As_{0.8-y}$ lattice matched to GaAs (Eq. 20.b) exhibits a trend comparable to that of $Ga_xIn_{1-x}N_ySb_{0.7}As_{0.3-y}$ lattice matched to GaSb (Eq. 16.b). These similarities suggest that the charge transfer properties in GaAs-matched alloys can be approximated using those of InAs- and GaSb-matched systems, which is valuable for predicting dielectric behavior in different lattice-matching conditions.

The computed ionicity and transverse effective charge in $Ga_xIn_{1-x}N_ySb_zAs_{1-y-z}$ alloys exhibit well-defined trends as a function of nitrogen content. The increasing ionicity with y highlights the role of nitrogen in modifying bond polarity, while the nonlinear behavior of e^*_T suggests complex charge redistribution effects at higher nitrogen concentrations. Furthermore, the observed similarities between the GaAs-lattice-matched alloys and those matched to InAs and GaSb provide valuable insights into the impact of composition on electronic properties, aiding in the design of materials for optoelectronic applications.

4. CONCLUSIONS

The dielectric constants and transverse effective charges of the pentanary alloy $Ga_xIn_{1-x}N_ySb_zAs_{1-y-z}$, lattice-matched to InAs, GaSb, and GaAs, have been systematically investigated using the pseudopotential approach within the virtual crystal approximation, combined with the Harrison bond-orbital model. The computed results exhibit reasonable agreement with available experimental data, validating the reliability of the adopted theoretical framework. However, just like other calculation models, our EPM-VCA-Harrison model has its limitations, especially in the detailed description of microscopic-scale effects such as the position of electronic states, local lattice distortions, as well as the disorder phenomena specific to multi-anionic alloys like GaInNAsSb.

Our analysis reveals that the dielectric constants and transverse effective charges exhibit distinct trends as a function of nitrogen composition (y), highlighting the significant influence of nitrogen incorporation on bond polarity and charge transfer mechanisms. Specifically, the ionicity increases nonlinearly with increasing nitrogen content due to its higher electronegativity, while the transverse effective charge follows a complex behavior, initially increasing before showing a downward curvature at higher (y) values. These trends underscore the interplay between electronic structure modifications and lattice distortions induced by compositional variations.

Moreover, the observed similarities between the dielectric properties of $Ga_xIn_{1-x}N_ySb_zAs_{1-y-z}$ alloys lattice-matched to different substrates (InAs, GaSb, and GaAs) suggest that the As/Sb ratio plays a crucial role in determining the bond character and charge redistribution. Such insights provide a predictive framework for optimizing these alloys for specific optoelectronic and electronic applications, where precise control over dielectric response and charge transport is required. Overall, our findings indicate that $Ga_xIn_{1-x}N_ySb_zAs_{1-y-z}$ is a promising material system for tailoring dielectric constants and transverse effective charges. These results open pathways for the design and discovery of new semiconductor materials with engineered dielectric and electronic properties, making them suitable for advanced applications in infrared optoelectronics, high-speed electronics, and photonic devices. Further experimental validation and computational studies incorporating many-body effects and strain considerations could refine these predictions and expand the applicability of these alloys.

Acknowledgments

The authors (T. Ghellab, Z. Charifi and H. Baaziz) would like to thank the general directorate for scientific research and technological development for their financial support during the realization of this work.

ORCID

Abid Hamza, https://orcid.org/0000-0001-9647-7425; **Baaziz Hakim,** https://orcid.org/0000-0003-4860-2740
Torkia Ghellab, https://orcid.org/0009-0001-6823-4335; **Zoulikha Charifi,** https://orcid.org/0000-0003-3875-4716

REFERENCES

[1] G. Li, *et al*. J. Mater. Chem. C, **12**, 12150 (2024). https://doi.org/10.1039/D4TC02615B
[2] S. Nakamura, J. Vac. Sci. Technol. A, **13**, 705 (1995). https://doi.org/10.1116/1.579811
[3] I. Vurgaftman, J.R.M. Meyer, and J.R. Ram-Mohan, J. Appl. Phys. **89**, 5815 (2001). http://dx.doi.org/10.1063/1.1368156
[4] K. Iga, and S. Kinoshita, *Process Technology for Semiconductor Lasers*, (Springer, Berlin, 1996).
[5] A.R. Kovsh, *et al*. Proc. of SPIE, **5349**, (2004). https://doi.org/10.1117/12.531245
[6] B. Merabet, A. Lachebi, and H. Abid, Turk. J. Phys, **35**(1), 13 (2011). https://doi.org/10.3906/fiz-0907-21
[7] H. Aourag, B. Bouhafs, and M. Certier, Phys. Stat. Sol (b), **201**, 117(1997). https://doi.org/10.1002/1521-3951(199705)201:1%3C117::AID-PSSB117%3E3.0.CO;2-8
[8] K. Kassali, and N. Bouarissa, Microelectron. Eng, **54**, 277 (2000). https://doi.org/10.1016/S0167-9317(00)00409-3

[9] H. Abid, N. Badi, M. Driz, N. Bouarissa, K. H. Benkabou, B. Khelifa, and H. Aourag, Microelectron. Eng B**, 33** 133 (1995).
[10] C. Skierbiszewski, P. Perlin, P. Wisniewski, W. Knap, T. Suski, W. Walukiewicz, W. Shan, *et al*. J. Appl. Phys, **76**, 2409 (2000). https://doi.org/10.1063/1.126360
[11] H.P. Xin, K.L. Kavanagh, M. Kondow, and C.W. Tu, J. Cryst. Growth, **201/202**, 419 (1999). https://doi.org/10.1016/S0022-0248(98)01366-9
[12] N. Bouarissa, H. Baaziz, Z. Charifi, Phys. Status Solidi, B: Basic Res, **231** 403 (2002). https://doi.org/10.1002/1521-3951(200206)231:2%3C403::AID-PSSB403%3E3.0.CO;2-6
[13] L. Vegard, Z. Phys. **5**, 17 (1921).
[14] T. Kobayasi, H. Nara, Bull. Coll. Med. Sci. Tohoku Univ, **2**, 7 (1993).
[15] H. Baaziz, Z. Charifi, and N. Bouarissa, Mater. Lett. **60**, 39 (2006). https://doi.org/10.1016/j.matlet.2005.07.067
[16] H. Mathieu, *Physique des semiconducteurs et des composants électroniques*, 5e éd., (Dunod, 2004).
[17] D.E. Aspnes, C.G. Olson, and D.W. Lynch, Phys. Rev. Lett, **37**, 766 (1976). https://doi.org/10.1103/PhysRevLett.37.766
[18] S. Adachi, J. Appl. Phys. **61**, 4869 (1987). https://doi.org/10.1063/1.338352
[19] S. Zollner, M. Garriga, J. Humlicek, S. Gopalan, and M. Cardona, Phys. Rev B, **43** 4349 (1991). https://doi.org/10.1103/PhysRevB.43.4349
[20] C. Alibert, A. Joullie, A.M. Joullie, and C. Ance, Phys. Rev. B, **27** 4946 (1983). https://doi.org/10.1103/PhysRevB.27.4946
[21] W.W. Walukiewicz, Physica E, **20** 300 (2004). https://doi.org/10.1016/j.physe.2003.08.023
[22] P.J.L. Herve, and L.K.J. Vandamme, Infrared Phys. Technol. **35**, 609 (1994). https://doi.org/10.1016/1350-4495(94)90026-4
[23] G.A. Samara, Phys. Rev. B, **27**, 3494 (1983). https://doi.org/10.1103/PhysRevB.27.3494
[24] S.Yu. Davydov, and S.K. Tikhonov, Semiconductors, **32**, 947 (1998). https://doi.org/10.1134/1.1187520
[25] P. Vogl, J. Phys. C: Solid State Phys, **11**, 251 (1978). https://doi.org/10.1088/0022-3719/11/2/011
[26] H. Baaziz, Z. Charifi, and N. Bouarissa, Mater. Chem. Phys. **68**, 197 (2001). https://doi.org/10.1016/S0254-0584(00)00352-7
[27] M. Levinshtein, S. Rumyantsev, and M. Shur, editors, *Handbook Series on Semiconductor Parameters*, vol. 2, (World Scientific, Singapore, 1999).
[28] P. Giannozzi, S. de Gironcoli, P. Pavone, and S. Baroni, Phys. Rev. B, 43, 7231 (1991). https://doi.org/10.1103/PhysRevB.43.7231
[29] V. Bougrov, M.E. Levinshtein, S.L. Rumyantsev, and A. Zubrilov, *Properties of Advanced Semiconductor Materials GaN, AlN, InN, BN, SiC, SiGe*, edited by M.E. Levinshtein, S.L. Rumyantsev, and M.S. Shur, (Wiley, New York, 2001), pp. 1–30.
[30] A. Zoroddu, F. Bernardini, P. Ruggerone, and V. Fiorentini, Phys. Rev. B, **64**, 045208 (2001). https://doi.org/10.1103/PhysRevB.64.045208
[31] T.L. Tansley, in: *Properties of Group III Nitrides*, edited by J.H. Edgar, (INSPEC, London, 1994).

ДІЕЛЕКТРИЧНІ КОНСТАНТИ ТА ПОПЕРЕЧНІ ЕФЕКТИВНІ ЗАРЯДИ У П'ЯТИКОМПОНЕНТНОМУ СПЛАВІ $Ga_xIn_{1-x}N_ySb_zAs_{1-y-z}$ З ҐРАТКОЮ, УЗГОДЖЕНОЮ З InAs, GaSb ТА GaAs

Х. Зеррухі[1], Х. Абід[1], Х. Баазіз[2,3], Т. Геллаб[2,3], З. Шаріфі[2,3]
[1]Лабораторія прикладних матеріалів, Дослідницький центр, Університет Сіді Бель Аббес, 22000 Алжир
[2]Кафедра фізики, Факультет природничих наук, Університет Мсила, 28000 Мсила, Алжир
[3]Лабораторія фізики та хімії матеріалів, Університет Мсила, Алжир

Це дослідження пропонує комплексний теоретичний аналіз діелектричних властивостей та поперечних ефективних зарядів п'ятикомпонентному сплаві $Ga_xIn_{1-x}N_ySb_zAs_{1-y-z}$, зосереджуючись на композиціях, ґратки яких узгоджені з підкладками InAs, GaSb та GaAs. У дослідженні використовується метод локального емпіричного псевдопотенціалу (EPM) у поєднанні з наближенням віртуального кристала (VCA) та моделлю зв'язків-орбіталей Гаррісона для оцінки ключових параметрів, включаючи статичну та високочастотну діелектричну константу, іонність, полярність та поперечний ефективний заряд. Ці обчислювальні підходи були обрані завдяки їхній здатності точно описувати електронні взаємодії в складних системах сплавів, зберігаючи при цьому обчислювальну ефективність. Отримані результати демонструють значну узгодженість з експериментальними даними, доступними для складових бінарних сполук, що підтверджує надійність теоретичної бази. Крім того, дослідження виявляє систематичні тенденції в діелектричній поведінці як функції складу, надаючи розуміння ролі атомного заміщення в налаштуванні цих властивостей. Наскільки нам відомо, ця робота являє собою першу детальну теоретичну оцінку сплавів $Ga_xIn_{1-x}N_ySb_zAs_{1-y-z}$ у цьому контексті. Хоча експериментальна перевірка залишається необхідною, наші результати встановлюють цінний теоретичний орієнтир для майбутніх досліджень та потенційних застосувань в оптоелектронній та напівпровідниковій приладобудуванні, зокрема в розробці передових інфрачервоних детекторів та високочастотних електронних компонентів.

Ключові слова: *EPM; полярність; діелектричні константи; поперечний ефективний заряд; сплави з узгодженою ґраткою; пентанарій*